Publisher: GSA
Journal: GEOL: Geology
Article ID: G35937

Ocean acidification in the aftermath of the Marinoan glaciation

Frank Ohnemueller[1,*], Anthony R. Prave[2], Anthony E. Fallick[3], and Simone A. Kasemann[1]

[1]*Department of Geosciences and MARUM - Center for Marine Environmental Sciences, University of Bremen, Leobener Str., D-28359 Bremen*

[2]*Department of Earth and Environmental Sciences, University of St Andrews, St Andrews KY16 9AL, UK*

[3]*Scottish Universities Environmental Research Centre, East Kilbride G75 0QF, UK*

*E-mail: FO: fohnemueller@marum.de

ABSTRACT

Boron isotope patterns preserved in cap carbonates deposited in the aftermath of the younger Cryogenian (Marinoan, ~635 Ma) glaciation confirm a temporary ocean acidification event on the continental margin of the southern Congo craton, Namibia. To test the significance of this acidification event and reconstruct Earth's global seawater pH states at the Cryogenian-Ediacaran transition we present a new boron isotope data set recorded in cap carbonates deposited on the Yangtze Platform in South China and the Karatau microcontinent in Kazakhstan. Our compiled $\delta^{11}B$ data reveal similar ocean pH patterns for all investigated cratons and confirm the presence of a global and synchronous ocean acidification event during the Marinoan deglacial period, compatible with elevated postglacial pCO_2 concentrations. Differences in the details of the ocean acidification event point to regional distinctions in the buffering capacity of Ediacaran seawater.

INTRODUCTION

During the Neoproterozoic era three major glacial sequences, namely the Sturtian (~716 Ma, Macdonald et al., 2010) the Marinoan (~635 Ma, Condon et al., 2005) and the Gaskiers

(~582 Ma, Hoffman and Li, 2009) resulted from modifications of global climate and biogeochemical cycles in response to changes to the ocean-continent-atmosphere interplay (e.g., Higgins and Schrag, 2003; Hoffman et al., 1998; Kirschvink, 1992). Predominant attention was focused on the Marinoan glaciation in efforts to establish global correlations between corresponding strata via comparable carbonate sequences, sedimentary structures and $\delta^{13}C$ patterns. (Hoffman and Schrag, 2002).

The aftermath of the Marinoan glaciation was associated with a marine transgression and the deposition of carbonate rocks, so-called *cap carbonates* or *cap dolomites*, which immediately overlie glacial deposits (Halverson et al., 2005; Hoffman et al., 1998; Hoffman and Schrag, 2002). These precipitates are interpreted as proxy archives of climatic and environmental changes characterizing the incipient deglacial phase (Hoffman et al., 1998). However, there is still an ongoing discussion about the atmospheric-oceanic conditions under which they were deposited, including ocean pH states (Kasemann et al., 2005; Kasemann et al., 2010) and continental weathering conditions (Higgins and Schrag, 2003; Hoffman et al., 1998; Kasemann et al., 2014; Silva-Tamayo et al., 2010). The significance and global nature of a temporary increase in the continental weathering flux following the demise of the Marinoan glaciation was recently recognized by calcium and magnesium isotope patterns preserved in cap carbonate rocks from Brazil, Canada and Namibia (Kasemann et al., 2014; Silva-Tamayo et al., 2010). To assess whether the proposed post-Marinoan ocean acidification event observed for the Congo craton in Namibia (Kasemann et al., 2010) is also of global extent or merely a regional manifestation, we present ocean pH reconstructions based on new boron ($\delta^{11}B$) isotope data from Marinoan-equivalent cap dolomite records of the Yangtze Platform in South China and the Kazakh Karatau microcontinent. Our new boron (and by deduction ocean pH) data in combination with

information on the weathering conditions allow to draw conclusions on atmospheric pCO_2, ocean-atmosphere CO_2 exchange and ocean alkalinities, and hence provide insights into habitable marine environments and ocean geochemical cycling during the Ediacaran.

GEOLOGICAL SETTING

Latest palaeogeographic reconstructions (e.g., Li et al., 2013) suggest that during the Cryogenian-Ediacaran transition all investigated cratons (Fig. 1 and Fig. DR1) were situated at low but ill-defined (up to 20° variance) latitudes. The southern Kazak Kyrshabakty Section (Fig. 1A, Karatau microcontinent) contains shallow water platform carbonates of the Kyrshabakty Formation from the Tamdy Series (e.g. Eganov et al., 1984). The inner shelf Northern Xiaofenghe Section (Three Gorges Area, Hubei Province, Fig. 1B) of the Yangtze Platform contains shallow water carbonates from the Doushantuo II Formation (Xiao et al., 2012). The stratigraphic framework and sedimentology of the Namibian Keilberg Member and Maieberg Formations of the Otavi Group in the shelf break Fransfontein Section and shallow water platform Ombaatjie and Khowarib Sections (Fig. 1C) are described in Kasemann et al. (2014). Details on all geological settings and their associated stratigraphy can be found within the Data Repository.

SAMPLE SELECTION AND ISOTOPE DATA

Prior to geochemical analyses, strict sample selection criteria were applied to obtain high-quality samples in which primary isotopic data are likely preserved. Sample selection and stable isotope analyses followed procedures detailed in Kasemann et al. (2005) and given in the Data Repository. Carbonate carbon ($\delta^{13}C_{carb}$), boron ($\delta^{11}B$) and oxygen ($\delta^{18}O$) isotope data of the investigated Kyrshabakty and N Xiaofenghe Section together with literature data of the Fransfontein, Khowarib and Ombaatjie Sections (Kasemann et al., 2010), are presented in Figure

2 and Table DR1 of the Data Repository. Unlike the Namibian sections, those from China and Kazakhstan are more condensed and not continuously exposed. We consequently focus on cap carbonates and the immediately overlying sedimentary units that record the B isotope excursions and the return to climate normalcy.

In detail, the $\delta^{11}B$ values for the Kyrshabakty Section display a sinusoidal profile and a relative shift of ~12‰. With the onset of cap dolomite deposition a steady decrease in $\delta^{11}B$ from 8.7 to 1.7‰ is recorded. The nadir of the negative excursion is situated 1.3 m above the glacial contact. Subsequently, the values continuously increase to 14.2‰ through the cap dolostone into the sandy dolostone unit and end with a lighter isotopic composition of 7.8‰ at 29.5 m. The Kyrshabakty Section carbonates record the typical negative $\delta^{13}C$ excursion for cap carbonate deposits worldwide (e.g. Halverson et al., 2005) represented by a decline from −0.1 to −2.8‰ and return toward positive values of 1.3‰ up section. The minimum value is located at 1.3 m as for the B isotopes; $\delta^{18}O$ data scatter around from −7.8 to −3.4‰. The bow shaped $\delta^{11}B$ profile for the Xiaofenghe Section starts with a value of 9.6‰ at 20 cm above the glacial deposit, declines to −2.2‰ at 1.6 m and returns to a maximum value of 14.8‰ within the sandy dolomites directly overlying the cap dolomites. $\delta^{13}C_{carb}$ data are in good agreement with literature data (Xiao et al., 2012), scatter around −4.0‰ within the cap carbonates and increase to 1.8‰ in the overlying sediments. $\delta^{18}O$ data show little scatter around −7.3 to −6.5‰.

As described by Kasemann et al. (2010) the $\delta^{11}B$ values of the Keilberg-Maieberg Formation display a prominent negative excursion, independent of lithology, facies settings or formation boundaries. The shallow water Khowarib and Ombaatjie Sections show relative $\delta^{11}B$ negative shifts of 11‰ and 9‰, respectively. $\delta^{11}B$ values at Ombaatjie Section start at 2.7‰, 10

cm above the base of the cap carbonates, decline to ~–6‰ in the Keilberg cap dolostones and return to positive values (~0‰) up section into the Maieberg limestones and dolostones. At the Khowarib Section $\delta^{11}B$ values start at 9.7‰ with the onset of cap carbonate precipitation, decline to –1.2‰ and return to ~3.2‰ from the Keilberg cap dolostones, through the Maieberg limestones and into the Maieberg dolostones. In contrast, the Fransfontein Section, representing a shelf break palaeo-environment, records a prolonged negative $\delta^{11}B$ excursion of ~11‰, reaching well above the Keilberg cap dolomites into the Maieberg Formation. The $\delta^{11}B$ profile starts at 3.0‰ when 20 cm into the Keilberg cap carbonates, decreases to –3.5‰ within the cap carbonates, and even to –4.3‰ though the Maieberg limestones into the Maieberg dolostones. Further up section the values climb back to 6.7‰ at the upper Maieberg dolostones. All investigated Namibian sections display the characteristic negative $\delta^{13}C_{carb}$ excursions with values down to –5.8‰. $\delta^{18}O$ varies widely from –0.9 to –11.4‰.

REGIONAL OCEAN pH PATTERN AND GLOBAL IMPLICATIONS

A prerequisite for accurate reconstruction of seawater pH from the B isotope composition of marine carbonates is the knowledge of the seawater B isotope composition ($\delta^{11}B_{sw}$), an unknown parameter for the Neoproterozoic. In analogy to Kasemann et al. (2010) and to infer ocean pH values for the aftermath of the Marinoan, we performed ocean pH calculations with a $\delta^{11}B_{sw}$ value of 20.5‰, using the empirical relationship between seawater pH and the B isotopic compositions of borate in solution and carbonates ($\alpha_{B3\text{-}B4}$ = 1.0272 at 25 °C from Klochko et al. (2006) and pK_B of 8.579 from Dickson (1990), see Data Repository for detailed description of palaeo pH reconstruction and assumed parameters).

In general, our new Chinese and Kazakh boron data are remarkably consistent with the Namibian data and show the same systematic negative $\delta^{11}B$ excursion and hence ocean pH patterns during the Marinoan deglacial phase, verifying the global extent of the ocean acidification event. The onset of cap carbonate deposition is characterized by positive $\delta^{11}B$ values and thus alkaline seawater with pH ~8.7. Within the cap dolomites, the decrease in $\delta^{11}B$ values leads into a temporary acidification event with minimum pH values of ~7 to ~8. Subsequently, the return to positive $\delta^{11}B$ values and thus more alkaline seawater conditions further up section is recorded. Enhanced atmospheric pCO_2 levels during the glaciation (Bao et al., 2008; Cao and Bao, 2013; Kasemann et al., 2005) and associated oceanic CO_2 uptake most likely triggered the global acidification event after the Marinoan ice age (Kasemann et al., 2010). The recovery from this ocean acidification event to alkaline pH conditions appears to be equally a global phenomenon that was associated with CO_2 drawdown by the globally enhanced continental weathering flux (Kasemann et al., 2014; Silva-Tamayo et al., 2010). The concomitant flux of alkalinity must have also enabled carbonate sedimentation even under acidic ocean conditions (Kasemann et al., 2014).

Also of global significance is the striking feature of alkaline ocean pH conditions at the onset of cap carbonate deposition that mirrors the inferred pH condition of the pre-glacial ocean and imposes interesting implications for the Neoproterozoic glacial environments and climate models (Kasemann et al., 2010). Simplistically, if ocean pH remained stable during glaciation and peak atmospheric CO_2 accumulation (Bao et al. 2008), a global sea-ice shield preventing air-sea gas exchange during glaciation needs to be inferred (Kasemann et al., 2010). The subsequent transition into ocean acidification may then have been triggered by the collapse of the global ice shield enabling the rapid oceanic uptake of CO_2. Alternatively, alkaline ocean pH condition at

the onset of cap carbonate deposition could have been caused by continental weathering and/or the development of a meltwater plume (Shields, 2005). An intense weathering pulse through highly reactive and quickly dissolving glacial rock flour (Le Hir et al., 2009) which was washed into the ocean, after continuous grinding of continental surfaces by ice sheet dynamics, might have buffered the seawater immediately after the glaciation and caused alkaline seawater conditions and high $\delta^{11}B$ values at the start of cap carbonate deposition. The influence on ocean pH via sea-ice and glacial meltwater injected into the Ediacaran Ocean, and possibly forming a widespread plume (e.g. Shields, 2005), is difficult to assess and such a plume could be alkaline or acidic. Following modern analogues of meltwater pools (e.g. Feely and Kleypas, 2012), dilution upon mixing with meltwater initially decreases the carbon content of seawater and increases its pH (to more alkaline conditions). As a consequence, the large pCO_2 disequilibrium between the surface ocean and atmosphere would drive oceanic CO_2 uptake and thus decrease ocean pH (as recorded in the ocean acidification pattern; for detailed descriptions see Data Repository).

Apart from the documented similarities in the $\delta^{11}B$-ocean pH relationship at the onset of deglaciation there are nevertheless significant differences in the acidification magnitude and duration not only between different continents (Fig. 2) but also within different facies along a single continental margin (Kasemann et al., 2010). The smallest drop in pH to a minimum of 8.2 is visible at the Kyrshabakty Section. After cap dolomite deposition, an overshoot to alkaline conditions of pH 9.1 is recorded within the directly overlying strata until a return to assumed ocean pH "normalcy" of ~8.7 takes place. The Xiaofenghe Section comprises a distinct negative peak in ocean pH down to 7.9. Similar to the Kyrshabakty Section, the recovery to a normal pH state takes place within the cap dolomites followed by an alkaline overshoot to pH ~9.1 in the

overlying Doushantuo II strata. A comparable pattern is obvious for the Namibian shallow water sections. The Ombaatjie Section hosts the most prominent ocean acidification of more than 1.6 pH units (nadir below pH 7). After this rapid decrease, a return to more alkaline pH states of ~8 is seen up section into the lowermost Maieberg Formation. At the Khowarib Section, the acidification by 0.8 pH units is less pronounced. The minimum pH is ~8 and the return to more alkaline seawater happens shortly after cap dolomite deposition within the lowermost Maieberg Formation. In contrast to the shallow water sections, the shelf break Fransfontein Section shows a distinctly different acidification duration with an ocean pH as low as 7.6 continuing until the middle Maieberg Formation, far above cap dolomite deposition.

Variations in seawater pH patterns within a single platform transect and between continents can operate on different time scales and be driven by several causes including varying weathering intensities, bathymetries, sedimentation rates and water temperatures. Kasemann et al. (2014) proposed that for the Namibian continental margin, ocean pH is influenced by rising ocean alkalinity through enhanced continental input fluxes, first in shallow water and most proximal environments, and later at the shelf break. Our new shallow water platform data from China and Kazakhstan support this proposal. All platform sections display a recovery from the acidification within or only shortly after cap dolomite deposition, in contrast to the shelf break environment where the recovery is significantly delayed. Furthermore, Namibian data indicate that the continental weathering flux transitioned from being of mixed carbonate and silicate character to a silicate-dominated one. Carbonate weathering would initially increase alkalinity and buffer pH, but only silicate weathering would drastically draw down atmospheric CO_2 (Higgins and Schrag, 2003; Kasemann et al., 2014). Hence, craton-specific variations in the continental weathering flux, together with regional distinctions in the timing of transition from

carbonate to silicate weathering and their respective magnitudes at the end of cap dolomite deposition, may have led to differences in pH patterns. If palaeo reconstructions (Fig. DR1, Li et al., 2013) are correct, variations in the acidification pattern could also arise from a diachronous ice-cover loss after glaciation (Hoffman and Li, 2009). Continents located near the equator should record the entire ocean acidification event including its recovery, whereas incomplete signals should be present polewards due to a delayed deposition. Instead, our data show a sharp synchronous negative $\delta^{11}B$ excursion and acidification pattern on each craton and therefore do not support such a scenario.

CONCLUSION

Our new results strongly support the assumption of a global ocean acidification event in the aftermath of the Marinoan glaciation as a potential consequence of oceanic CO_2 uptake. Ocean acidification was most probably ended by CO_2 drawdown via globally enhanced continental weathering as indicated by Higgins and Schrag (2003), Kasemann et al. (2014) and Silva-Tamayo et al. (2010). At the immediate deglacial phase, alkaline ocean pH conditions (similar to the incipient glaciation) are recorded. Global sea-ice cover preventing CO_2 ocean-atmosphere exchange during glaciation, seawater dilution by sea-ice and glacial meltwater or a massive weathering flux by glacial rock flour (Le Hir et al., 2009), could each have been the reason. While all investigated cratons show similar and largely synchronous seawater pH patterns, regional differences in minimum pH values, as well as in magnitudes and acidification durations are recorded. It appears that platform facies display a faster return to normal ocean pH conditions than shelf break facies as a direct consequence of the massive alkalinity flux to the ocean and hence increased buffer capacity leading to more alkaline seawater.

ACKNOWLEDGMENTS

This work was funded by the DFG to SAK as part of the FOR 736. We thank U. Struck and A. Gamper (Museum für Naturkunde, Berlin) for providing $\delta^{13}C$ and $\delta^{18}O$ data from Kazakhstan and China. We are grateful to S. Pape (University of Bremen) for trace element measurements, to C. Vogt (University of Bremen), R. Oeser and D. Hippler (TU Berlin) for XRD analyses. Thanks to F. Lucassen and A. Meixner for useful discussions. This manuscript has greatly benefited from the constructive comments of John Higgins and Paul Hoffman. Fieldwork in China was supported by the NSFC. Fieldwork in Kazakhstan was guided by G. Yergaliev and S. Zhemzhushnikov (Kazakh Academy of Sciences).

REFERENCES CITED

Alexeiev, D.V., Cook, H.E., Buvtyshkin, V.M., and Golub, L.Y., 2009, Structural evolution of the Ural-Tian Shan junction: A view from Karatau ridge: South Kazakhstan: Comptes Rendus Geosciences, v. 341, no. 2–3, p. 287–297.

Bao, H., Lyons, J.R., and Zhou, C., 2008, Triple oxygen isotope evidence for elevated CO_2 levels after a Neoproterozoic glaciation: Nature, v. 453, no. 7194, p. 504–506, doi:10.1038/nature06959.

Cao, X.B., and Bao, H.M., 2013, Dynamic model constraints on oxygen-17 depletion in atmospheric O-2 after a snowball Earth: Proceedings of the National Academy of Sciences of the United States of America, v. 110, no. 36, p. 14546–14550.

Condon, D., Zhu, M., Bowring, S., Wang, W., Yang, A., and Jin, Y., 2005, U-Pb Ages from the Neoproterozoic Doushantuo Formation, China: Science, v. 308, no. 5718, p. 95–98, doi:10.1126/science.1107765.

Cremonese, L., Shields-Zhou, G., Struck, U., Ling, H.-F., Och, L., Chen, X., and Li, D., 2013, Marine biogeochemical cycling during the early Cambrian constrained by a nitrogen and

organic carbon isotope study of the Xiaotan section, South China: Precambrian Research, v. 225, p. 148–165, doi:10.1016/j.precamres.2011.12.004.

Dickson, A.G., 1990, Thermodynamics of the dissociation of boric acid in synthetic seawater from 273.15 to 318.15 K: Deep-Sea Research. Part A: Oceanographic Research Papers, v. 37, no. 5, p. 755–766, doi:10.1016/0198-0149(90)90004-F.

Eganov, E.A., Ergaliev, G.K., Ilyin, A.V., and Krasnov, A.A., 1984, Guidebook / International Geological Congress, XXVII Session Kazakhstan: Karatau Phosphorite Basin, Moskau, Nauka.

Feely, R. A., and Kleypas, J., 2012, Will melting ice caps dilute the acidity by adding freshwater to the ocean, *in* Cooley, S., Mathis, J., Yates, K., Turley, C., eds., Frequently Asked Questions about Ocean Acidification: U.S. Ocean Carbon and Biogeochemistry Program and the UK Ocean Acidification Research Programme, Version 2, www.whoi.edu/OCB-OA/FAQs

Halverson, G.P., Hoffman, P.F., Schrag, D.P., Maloof, A.C., and Rice, A.H.N., 2005, Toward a Neoproterozoic composite carbon-isotope record: Geological Society of America Bulletin, v. 117, no. 9–10, p. 1181–1207, doi:10.1130/B25630.1.

Higgins, J.A., and Schrag, D.P., 2003, Aftermath of a snowball Earth: Geochemistry Geophysics Geosystems, v. 4, no. 3, doi:10.1029/2002GC000403.

Hoffman, P.F., and Li, Z.-X., 2009, A palaeogeographic context for Neoproterozoic glaciation: Palaeogeography, Palaeoclimatology, Palaeoecology, v. 277, no. 3–4, p. 158–172, doi:10.1016/j.palaeo.2009.03.013.

Hoffman, P.F., and Schrag, D.P., 2002, The snowball Earth hypothesis: Testing the limits of global change: Terra Nova, v. 14, no. 3, p. 129–155, doi:10.1046/j.1365-3121.2002.00408.x.

Hoffman, P.F., Kaufman, A.J., Halverson, G.P., and Schrag, D.P., 1998, A Neoproterozoic Snowball Earth: Science, v. 281, no. 5381, p. 1342–1346, doi:10.1126/science.281.5381.1342.

Kasemann, S.A., Hawkesworth, C.J., Prave, A.R., Fallick, A.E., and Pearson, P.N., 2005, Boron and calcium isotope composition in Neoproterozoic carbonate rocks from Namibia: Evidence for extreme environmental change: Earth and Planetary Science Letters, v. 231, no. 1–2, p. 73–86, doi:10.1016/j.epsl.2004.12.006.

Kasemann, S.A., Prave, A.R., Fallick, A.E., Hawkesworth, C.J., and Hoffmann, K.-H., 2010, Neoproterozoic ice ages, boron isotopes, and ocean acidification: Implications for a snowball Earth: Geology, v. 38, no. 9, p. 775–778, doi:10.1130/G30851.1.

Kasemann, S.A., Pogge von Strandmann, P.A.E., Prave, A.R., Fallick, A.E., Elliott, T., and Hoffmann, K.-H., 2014, Continental weathering following a Cryogenian glaciation: Evidence from calcium and magnesium isotopes: Earth and Planetary Science Letters, v. 396, no. 0, p. 66–77, doi:10.1016/j.epsl.2014.03.048.

Kirschvink, J.L., 1992, Late Proterozoic Low-Latitude Global Glaciation: The Snowball Earth: Section 2.3, *in* Schopf, J.W., Klein, C., and Des Maris, D., eds., The Proterozoic Biosphere: A Multidisciplinary Study: Cambridge, Cambridge University Press, p. 51–52.

Klochko, K., Kaufman, A.J., Yao, W., Byrne, R.H., and Tossell, J.A., 2006, Experimental measurement of boron isotope fractionation in seawater: Earth and Planetary Science Letters, v. 248, no. 1–2, p. 276–285, doi:10.1016/j.epsl.2006.05.034.

Le Hir, G., Donnadieu, Y., Goddéris, Y., Pierrehumbert, R.T., Halverson, G.P., Macouin, M., Nédélec, A., and Ramstein, G., 2009, The snowball Earth aftermath: Exploring the limits of

continental weathering processes: Earth and Planetary Science Letters, v. 277, no. 3–4, p. 453–463, doi:10.1016/j.epsl.2008.11.010.

Li, Z.-X., Evans, D.A.D., and Halverson, G.P., 2013, Neoproterozoic glaciations in a revised global palaeogeography from the breakup of Rodinia to the assembly of Gondwanaland: Sedimentary Geology, v. 294, no. 0, p. 219–232, doi:10.1016/j.sedgeo.2013.05.016.

Macdonald, F.A., Schmitz, M.D., Crowley, J.L., Roots, C.F., Jones, D.S., Maloof, A.C., Strauss, J.V., Cohen, P.A., Johnston, D.T., and Schrag, D.P., 2010, Calibrating the Cryogenian: Science, v. 327, no. 5970, p. 1241–1243, doi:10.1126/science.1183325.

Shields, G., 2005, Neoproterozoic cap carbonates: a critical appraisal of existing models and the plumeworld hypothesis: Terra Nova, v. 17, no. 4, p. 299-310, doi:10.1111/j.1365-3121.2005.00638.x.

Silva-Tamayo, J.C., Nägler, T.F., Sial, A.N., Nogueira, A., Kyser, K., Riccomini, C., James, N.P., Narbonne, G.M., and Villa, I.M., 2010, Global perturbation of the marine Ca isotopic composition in the aftermath of the Marinoan global glaciation: Precambrian Research, v. 182, no. 4, p. 373–381, doi:10.1016/j.precamres.2010.06.015.

Xiao, S., McFadden, K.A., Peek, S., Kaufman, A.J., Zhou, C., Jiang, G., and Hu, J., 2012, Integrated chemostratigraphy of the Doushantuo Formation at the northern Xiaofenghe section (Yangtze Gorges, South China) and its implication for Ediacaran stratigraphic correlation and ocean redox models: Precambrian Research, v. 192–195, no. 0, p. 125–141, doi:10.1016/j.precamres.2011.10.021.

FIGURE CAPTIONS

Figure 1. A: Geological sketch of the Malyi and Bolshoi Karatau Range displaying the study area east of Zhanatas (modified after Alexeiev et al., 2009). B: Generalized map of the Chinese

Yangtze Platform including the northern Xiaofenghe Section, Hubei Province (modified after Cremonese et al., 2013). C: Generalized geological map of northern Namibia showing the locations of the Fransfontein, Ombaatjie and Khowarib Sections (modified after Kasemann et al., 2010).

Figure 2. Stratigraphic column of the investigated sections with corresponding $\delta^{11}B$ (‰) and $\delta^{13}C_{carb}$ (‰) isotope data and estimated ocean pH. The gray shaded area marks the cap carbonates. A: Kyrshabakty Section, Malyi Karatau microcontinent, Kazakhstan. B: Northern Xiaofenghe Section, Yangtze Platform, South China. C: Ombaatjie Section, Congo craton, Namibia. D: Khowarib Section, Congo craton, Namibia. E: Fransfontein Section, Congo craton, Namibia. AT - Aktas tillite, NT - Nantuo tillite, GG - Ghaub glacial deposit, KF - Keilberg Formation.

[1]GSA Data Repository item 2014xxx, detailed information of the geological setting, methods, sample selection, evaluation of post depositional alteration, and ocean pH reconstruction, is available online at www.geosociety.org/pubs/ft2014.htm, or on request from editing@geosociety.org or Documents Secretary, GSA, P.O. Box 9140, Boulder, CO 80301, USA.

Figure1

Click here to download Figure: figure1.pdf

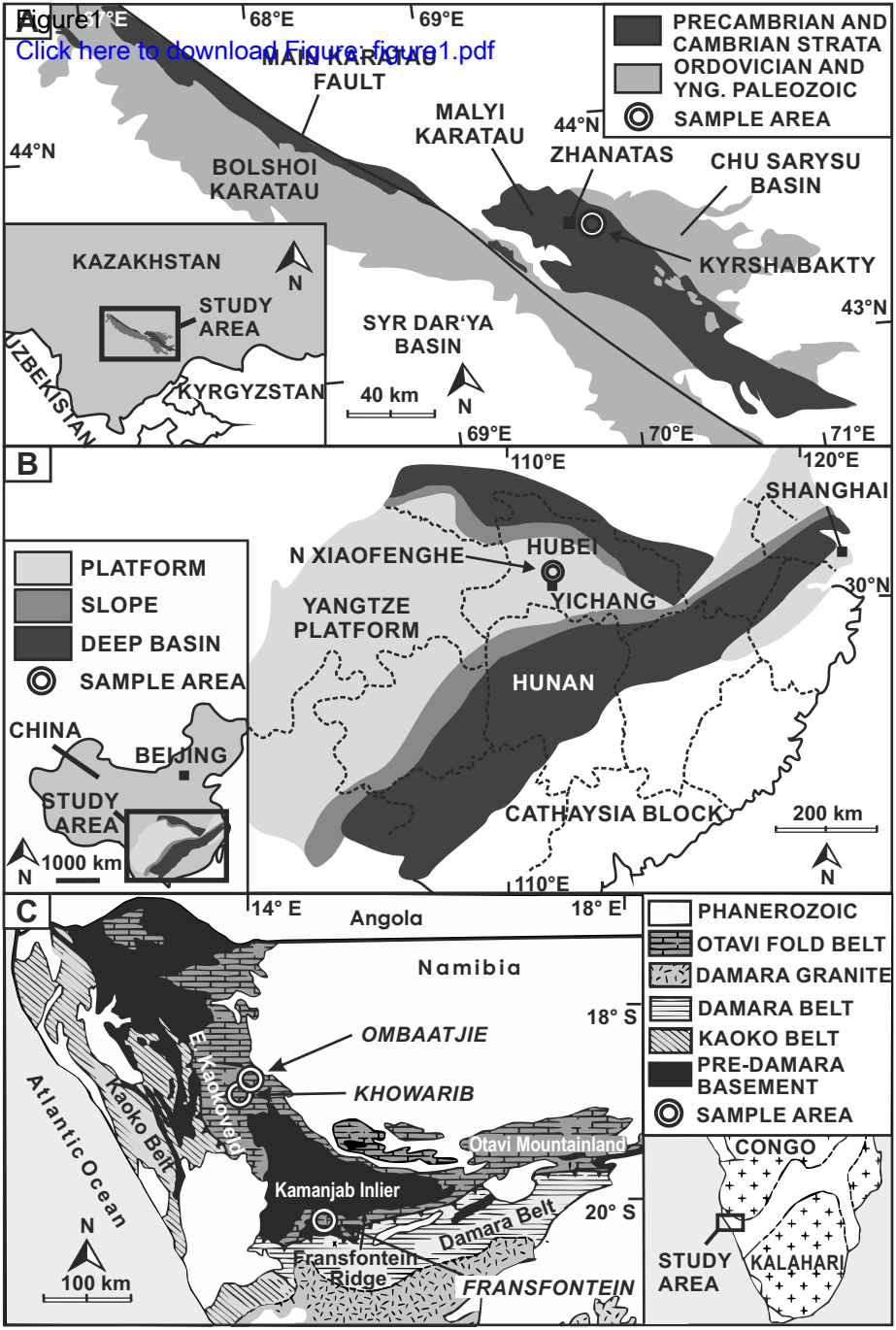

Figure2

Click here to download Figure: figure2.pdf

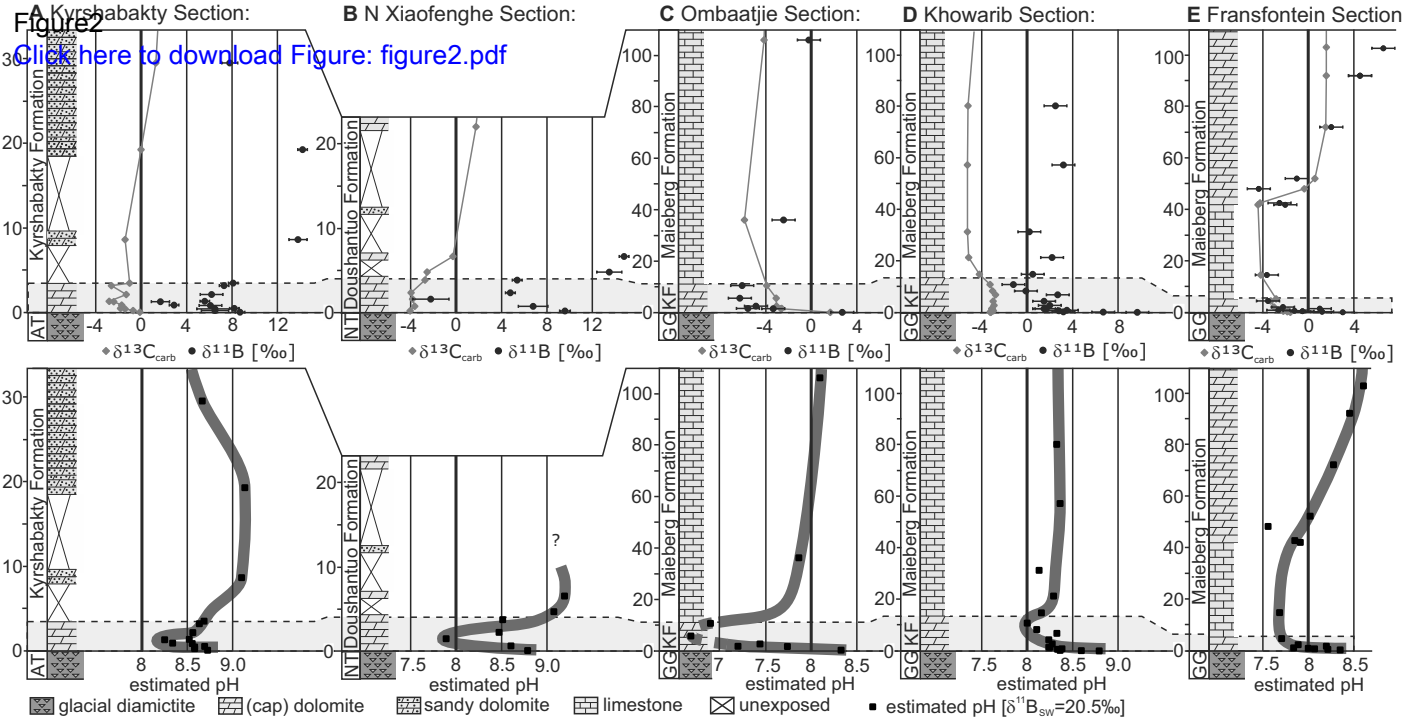

Supplement

Ocean acidification in the aftermath of the Marinoan glaciation

Frank Ohnemueller, Anthony R. Prave, Anthony E. Fallick, Simone A. Kasemann

GEOLOGICAL SETTING

Yangtze Platform (China)

Precambrian-Cambrian strata are widespread on the Yangtze Platform (Zhang et al., 1997; Zhu et al., 2003). The Three Gorges area is located at the central northern part of the platform, Hubei Province. Platform interior successions are typically comprised of shallow-water carbonates and deep-water shales of Cryogenian to Cambrian age. From oldest to youngest, the Liantuo, Nantuo, Doushantuo, Dengying, Yanjiahe, Shuijingtuo and Shipai Formations (Ma et al., 1984) are exposed in the Three Gorges area. The investigated Xiaofenghe Section (N 30°56.491, E 111°13.957) is located approximately 28 km N of Yichang, crops out along the northern and southern mountainsides of a small valley, and provides access to ~200 m of well exposed strata.

Nantuo Formation glacial diamictites are directly overlain by ~4 m of Doushantuo Formation cap dolomites (Doushantuo I), which can be subdivided by microfacies into C1, C2 and C3 after the classification of Jiang et al. (2003). The lowermost 0.5 m correspond to unit C1 and consist of grey dolostones with minor calcite veining. Up to ~2.5 m a grey, fine laminated, micritic dolostone (C2) with minor cm-scale chert layers is exposed. The uppermost unit (C3) displays a laminated dolostone layer containing teepee-like fluid-escape structures. On top of the cap dolomite are several meters of grey, micritic dolostones interbedded with chert-nodule-

bearing black shales (Doushantuo II Formation). Xiao et al. (2012) suggested the northern Xiaofenghe Section represented a shallow-water, inner shelf environment.

Karatau microcontinent (Kazakhstan)

The southern Kazakh Karatau Mountains form the foothills of the Tian Shan orogen and consist of the Bolshoi (NW) and Malyi (SE) Karatau Range that are divided by the Main Karatau Fault (Alexeiev et al., 2009 and references therein). The investigated Kyrshabakty Section (N 43°32'2.1" E 69°57'7.7"), located approximately 18 km E of Zhanatas is part of the Malyi Karatau Range which is surrounded by the Syr Dar'ya Basin to the SW and the Chu Sarysu Basin to the NE (Allen et al., 2001). The complete Precambrian-Cambrian succession is described in detail by Eganov et al. (1984) and Meert et al. (2011). We focused on the lowermost Kyrshabakty Formation which is part of the Tamdy Series and comprises a ~45 m thick diamictite layer (Aktas tillite) overlain by ~3.5-4 m thick cream-to-ivory-colored cap dolomites without any noticeable sedimentary features besides a fine lamination. Up section, the succession is marked by alternation of dolomitic sandstones and sandy dolostones with an increasing trend in dolomite content towards the top. The first ~30 m of the section are defined by a transgressive system tract and the palaeoenvironment is suggested to represent a very shallow water platform setting which is also confirmed by Eganov et al. (1986).

Congo craton (Namibia)

The analyzed marine successions were all situated on the low-latitude (Fig. DR1) continental margin of the southern Congo craton and comprise Neoproterozoic to Cambrian rocks. We concentrate on the thick sequence of carbonate rocks corresponding to the Tsumeb Subgroup, being part of the Otavi Group (Hoffmann et al., 2004; Kaufman et al., 1991). In detail, the shallow-marine platform Ombaatjie and Khowarib Sections as well as the shelf break Fransfontein Section (see Fig. 1 manuscript) provide access to Ghaub glacial deposits (~635

Ma, Hoffmann et al., 2004) overlain by post-glacial Keilberg Member cap dolomites transitioning into a >100 m thick succession of Maieberg Formation dolo- and limestones (Hoffman et al., 1996; Kasemann et al., 2010; Kaufman et al., 1991). The cap carbonates are micritic dolostones, which can be subdivided into a basal laminated unit, a middle unit containing soft-sediment deformation, sheet-cracks and stromatolite structures and a capping interval of thin-bedded dolostones. The Maieberg Formation is comprised of rhythmite limestones and thin-bedded dolo- and limestones at the Khowarib and Ombaatjie Section and only of thin-bedded dolostones at the Fransfontein Section (Kasemann et al., 2010). A more detailed stratigraphy and overview about the large-scale tectonic situation is provided e.g. by Miller (2008).

SAMPLE SELECTION CRITERIA / ALTERATION EVALUATION

Sample selection and quality evaluation for the Namibian carbonate dataset is described in Kasemann et al. (2010). Fresh rock hand samples of the Kyrshabakty Formation (Kazakhstan) and the Doushantuo Formation (South China) carbonates were taken in 10-30 cm intervals and selected by their uniformity and absence of any obvious alteration or veining. To assure a good sample quality, we checked the samples macroscopically in the field, afterwards microscopically in the lab (thin section, scanning electron microscopy) and performed geochemical tests (trace element and oxygen isotope analyses). Rock powders were prepared from pre-screened, micritic, cleaned and fresh surface rock chips with an agate vibratory disc mill at the Museum für Naturkunde Berlin, Germany.

METHODS

Boron measurements

Boron ($\delta^{11}B$) isotope analyses were performed by the method detailed in Kasemann et al. (2001). For analyses, 10 mg of the sample powder was dissolved in 100 µl 1 N HCl for 24 h at

20°C and subsequently centrifuged. The $n(^{11}B)/n(^{10}B)$ measurements were performed on a Thermo Fisher Scientific TRITON *Plus* mass spectrometer, using negative thermal ionization mass spectrometry (N-TIMS). 1 µl boron-free seawater emitter (Vogl et al., 2011) was placed on a degassed Re single filament and dried at 0.7 A. Subsequently, 1 µl of the sample solution containing ~1 ng B was added, evaporated to complete dryness at 0.7 A and afterwards heated at 1.2 A for 30 s. Boron isotopes were registered as BO_2^- complexes on masses 42 and 43, and measurements were carried out at 970°-1050°C with an ion beam intensity of 3-30 pA on mass 43. Each measuring procedure consisted of up to 200 blocks with 10 cycles, taking about 3 hours of data acquisition. To correct for a CNO^- interference on mass 42 occurring at the beginning of some measurements and for isotopic fractionation during analysis, the extrapolation technique described by Kasemann et al. (2001) was used during data evaluation.

Boron isotope ratios are given in $\delta^{11}B$-notation relative to the certified reference material NIST SRM 951 that showed an $^{11}B/^{10}B$ ratio of 4.0068±0.0016 (2sd=0.4‰, n=37 over a period of 12 month). In addition to the NIST material, the standard material M93-TB-FC-1, a *Porites* coral with a published value of 24.8±0.4‰ ($2\sigma_{mean}$), as determined by different multicollector techniques (Kasemann et al., 2009), was also regularly analyzed. The coral replicates gave $\delta^{11}B$ of 24.1±0.7‰ (2sd, n=16). Samples were analyzed at least twice and their reproducibility (2sd) is given in Table DR1.

Carbon and oxygen measurements

The $\delta^{13}C_{carb}$ and $\delta^{18}O$ isotope dataset is based on 14 bulk rock samples of the Kyrshabakty Section and 9 samples of the Xiaofenghe Section, respectively. All measurements were carried out on a Thermo Finnigan GASBENCH II linked online to a Thermo Finnigan DELTA V isotope ratio mass spectrometer at the Museum fuer Naturkunde Berlin, Germany. Isotope ratios are reported in δ-notation in [‰] relative to the Vienna Peedee Belemnite (VPDB). The analytical reproducibility of $\delta^{13}C_{carb}$ and $\delta^{18}O$ values is each generally better than ±0.2‰ (2sd).

Trace element analyses

Trace elements analyses (Table DR2) of the northern Xiaofenghe Section carbonates were performed on an Agilent Technologies 700 Series ICP-OES at the inorganic geochemistry group of the MARUM, Germany. Three replicates of each dilution/concentration were measured and typically had a relative standard deviation (RSD) of better than 3% (excepting boron, which was < 7%).

Clay contamination

To avoid contamination by the dissolution of boron-bearing clays during chemical preparation a 1N HCl (100 µl 1 N HCl for 10mg of sample powder) is used during the dissolution procedure. Dissolution of B-bearing clays would generally increase the boron concentration. Potential modification of the isotope composition is dependent on the clay source and hence difficult to assess, but is expected to be negligible due to a similar fractionation factor between seawater - carbonates and seawater - clay (Palmer et al., 1987). To assess the amount of clay in the sample material XRD analyses of Kyrshabakty Formation cap dolomites were performed at the Mineralogy Department of the Technical University Berlin, Germany. A semi-quantitative data evaluation after Cook et al. (1975) showed an average clay content <1%. XRD analyses of the Chinese data set done at the ZEKAM, University of Bremen, Germany showed average clay content of ~6%. To test for clay contamination in the sample solution, trace element analyses were performed on an Agilent Technologies 700 Series ICP-OES at the inorganic geochemistry group, University of Bremen, Germany. The boron concentration is 2 µg g^{-1} without any obvious correlation to varying clay content. For example, Al concentrations are around 200 ppm (Table DR2) and are not correlated to the B concentration (R =0.22). In addition, there is no correlation of boron concentration and boron isotope values at the 95% significance level (R =0.46). Hence boron contamination by clay dissolution can be excluded.

Post-depositional alteration

Post-depositional alteration, especially diagenesis, is thought to decrease the isotopic composition of oxygen, boron and carbon isotopes (Derry et al., 1992; Kaufman et al., 1993; Paris et al., 2010; Veizer et al., 1999). On that account, only samples with $\delta^{18}O$ values > -10‰ are considered to be of primary origin and suitable for further isotope analyses. Doushantuo Formation dolomites show average $\delta^{18}O$ values of -6.8‰ with no $\delta^{18}O$ value lower than -7.3‰ and without any significant correlation at the 5% significance level (R =0.22) to the carbon (Fig. DR2) or boron isotopic composition. A similar situation holds with respect to the Kyrshabakty Formation data. The average $\delta^{18}O$ value is -5‰ and as per the Chinese data there is no significant or obvious correlation with $\delta^{13}C$ at the 5% significance level (R =0.07, Fig. DR2) or with $\delta^{11}B$ data. Further, both the $\delta^{18}O$ and $\delta^{13}C$ are in perfect agreement with literature data for that time (e.g. Jacobsen and Kaufman, 1999). Diagenesis is also thought to cause a correlation between the boron concentration and the $\delta^{11}B$ values (Spivack and You, 1997). However, no relationship is obvious for our data set.

For the Phanerozoic, primary isotopic signals recorded by carbonates are expected to show Mn/Sr ratios below 10. In comparison, Mn/Sr values above 10 are present in China, which could be a result of hydrothermal overprint, as suggested for the Doushantuo Formation (Derkowski et al., 2013). However, enriched Mn/Sr are a common feature of cap dolomites and also reported by e.g. Liu et al. (2013). In general, the reliability of Mn/Sr ratios as an alteration criterion is doubted for Neoproterozoic rocks by many authors. This is due to its being strongly dependent on the primary precipitated carbonate mineral phase (Derry, 2010), and high Mn/Sr ratios can also result from precipitation in early diagenetic anoxic waters (Miller et al., 2009), potentially present during the time of cap dolomite deposition. Also, increased seawater concentrations of Mn and Fe (see Table DR2) leading to high Mn/Sr during the Marinoan time interval are likely, due to the potential absence of abundant oxygen and sulfate necessary for redox reactions

(Anbar and Knoll, 2002; Hoffman and Li, 2009; Miller et al., 2009; Raub et al., 2007). We therefore conclude that our boron isotope data have not been diagenetically compromised. In addition, systematic cyclical isotopic patterns at all measured sections and on different continents further supports interpreting the isotopic signatures as primary values.

CONSTRAINTS ON OCEAN pH RECONSTRUCTION

In seawater two dominant boron species are present: boric acid ($B(OH)_3$) and borate-ion ($B(OH)_4^-$) (Kakihana et al., 1977; Spivack and Edmond, 1987). Between these two species an isotopic exchange (Hemming and Hanson, 1992) is described by the reaction displayed in equation [1]:

$$^{11}B(OH)_3 + {}^{10}B(OH)_4^- <=> {}^{10}B(OH)_3 + {}^{11}B(OH)_4^- \quad [1]$$

Due to the fact that the abundance of the species and their isotopic composition is pH dependent and marine carbonates predominantly incorporate the charged, tetrahedral species (Hemming and Hanson, 1992; Sanyal et al., 2000), palaeo pH calculations by boron isotope measurements are possible (Klochko et al., 2006), with the relationship given in equation [2]:

$$pH = pK_B - \log\left[- \frac{\delta^{11}B_{SW} - \delta^{11}B_{carb}}{\delta^{11}B_{SW} - \alpha_{B3\text{-}B4} \cdot \delta^{11}B_{carb} - 1000 \cdot (\alpha_{B3\text{-}B4} - 1)} \right] \quad [2]$$

To calculate seawater pH, we need the B isotope composition of the carbonate ($\delta^{11}B_{carb}$) and the seawater ($\delta^{11}B_{sw}$) (discussed below), as well as the isotope fractionation factor for boron ($\alpha_{B3\text{-}B4}$) and the dissociation constant of boric acid (pK_B), both of which are temperature dependent. To infer ocean pH values and compare the pH patterns of the different continents, we performed ocean pH calculations with a $\delta^{11}B_{sw}$ value of 20.5‰ (see below) using the empirical fractionation factor for seawater pH and the B isotopic compositions of borate in solution and carbonates of $\alpha_{B3\text{-}B4} = 1.0272$ (Klochko et al., 2006), and a pK_B of 8.579 (Dickson, 1990) both for 25°C seawater temperature. Since exact seawater temperatures for the Early

169 Ediacaran are unknown we have to rely on modelled values. Initial seawater temperatures
170 of -1.5°C rapidly increasing to ~30°C after the deglacial are modelled by Higgins and Schrag
171 (2003). Variations in sea surface temperatures between 15°C and 35°C, most likely reflecting
172 the temperatures prevailing during platform carbonate precipitation, would result in a maximum
173 difference of < 0.2 pH. Generally, colder temperatures lead to slightly higher pH conditions,
174 whereas warmer seawater temperatures lead to slightly more acidic conditions. For our dataset,
175 the relative ocean pH pattern including the acidification magnitudes would stay completely the
176 same.

177 The pK_B also changes with different salinities (Dickson, 1990). However, even if lower
178 salinities (S= ~25 ppt) are assumed due to meltwater influx (Shields, 2005) the associated
179 isotopic variations are negligible for our dataset and a salinity assumption of S = 35 ppt is used
180 for calculations.

181 Modern seawater is taken as homogeneous with a $\delta^{11}B_{sw}$ of 39.6‰ (e.g. Foster et al., 2010). In
182 the past, significant variations in $\delta^{11}B_{sw}$ are likely and attributed to changes in the global boron
183 budget (Joachimski et al., 2005). The residence time of boron in the modern ocean is ~14-20
184 Ma (Lemarchand et al., 2000; Spivack, 1986) and should be roughly similar during the
185 Neoproterozoic, but is in any case far higher than the maximal assumed duration of cap
186 carbonate deposition (~3 Ma, Condon et al., 2005). Consequently, ocean-pH changes instead
187 of variations in seawater $\delta^{11}B$ composition are recorded at the investigated sections. To gauge
188 ocean pH conditions in the Neoproterozoic, Kasemann et al. (2005) initially explored different
189 pH profiles with basic and acidic end-members. Subsequently, Kasemann et al. (2010) opted
190 for slightly acidic seawater conditions, based on pH models for the Precambrian (Grotzinger
191 and Kasting, 1993; Higgins and Schrag, 2003) and calculated relative ocean pH variation of as
192 much as 1.5 pH units based on $\delta^{11}B_{sw}$ values between 20‰ and 23‰. By combining our new
193 Chinese and Kazakh dataset together with the already published Namibian literature data, we

suggest and use a seawater composition of 20.5‰ as our 'best-guess' value. Using a higher isotope composition for the seawater, unlikely acidic conditions (< pH 6) for the acidification event would result for some sections, while assumed lower $\delta^{11}B_{sw}$ would lead to highly alkaline seawater conditions (> pH 9.5). In comparison to models and calculations for that time (e.g. Higgins and Schrag, 2003; Kempe and Kazmierczak, 2002), we regard each as unlikely. For a better comparison and overview, we nevertheless performed ocean pH calculations for different $\delta^{11}B$ seawater assumptions (A: 20.5‰, B: 21.5‰, and C: 22.5‰) summarized in Table DR1. The overall acidification pattern observed at all sections is only negligibly affected by changes to the boron isotope seawater composition. For the Ombaatjie Section a pH calculation is only possible with model A, due to its very low boron isotope ratios (note that the uncertainty of the isotope value is ~1‰ ($2\sigma_f$) for the Ombaatjie Section).

We evaluate the observed initial and maximum differences in seawater pH (~1 pH unit) between the investigated sections as reasonable, especially in respect of modern large-scale open ocean surface water pH measurements showing variation >0.5 pH (Doney, 2006; Takahashi et al., 2014). Even larger differences must be expected on local to regional scale and ocean pH in fact differs on a daily and monthly basis (Hofmann et al., 2011). Additionally, local and regional differences in seawater pH between different sample localities can result from e.g. upwelling, riverine influx, productivity regimes and alkalinity states (Kisakurek et al., 2005; Pearson and Palmer, 2000; Takahashi et al., 2014).

ALTERNATIVE MODELS FOR A POSTGLACIAL ALKALINE OCEAN AND A SUBSEQUENT OCEAN ACIDIFICATION

As mentioned in the manuscript, different explanations may exist for alkaline ocean pH condition at the onset of cap carbonate deposition. Apart from assuming a global ice shield preventing air-sea gas exchange during glaciation, a continental weathering pulse at the beginning of deglaciation (Le Hir et al., 2009) and/or the development of a meltwater plume

(Shields, 2005) could each serve as reasons. Highly reactive and quickly dissolving glacial rock flour (Le Hir et al., 2009) produced during continuous grinding of continental surfaces by ice sheet dynamics could have been washed into the ocean causing an intense weathering pulse that might have buffered the seawater immediately after the glaciation and caused alkaline seawater conditions and high $\delta^{11}B$ values at the start of cap carbonate deposition. To assess the potential influx and buffering capacity of glacial rock flour, additional proxy data that respond to weathering over short timescales are needed. Alternatively, sea-ice and glacial meltwater injected into the ocean could have led to the evolution of a widespread meltwater plume and could have affected the pH of the surface ocean. Recent studies on meltwater demonstrate a highly variable CO_2-carbonate chemistry together with significant differences in pH values of meltwater from ~5 to >10 including supraglacial and subglacial meltwater drainage, glacial rivers, melt ponds, deposited snow, brines and sea ice (Bates et al., 2014; e.g. Hare et al., 2013; Larose et al., 2010; Singh et al., 2012; Tegt, 2002). These tremendous differences in pH are controlled by e.g. CO_2 uptake from the atmosphere, sea ice freezing processes, host rock compositions below the glaciers and varying chemical weathering rates (Wimpenny et al., 2010) and make it difficult to predict the balance and dynamics of ocean pH in today's high latitude world (Bates et al., 2014), and to even assess the pH influence of meltwater influx into the postglacial Ediacaran ocean. In a recent study, Feely and Kleypas (2012) performed a mass-balance modeling of a situation involving melting of the Arctic and Antarctic ice caps, probably the best approximate to the post-Marinoan meltwater plume hypothesis described by e.g. Liu et al. (2014) and Shields (2005). They suggest an initial increase in seawater pH due to the enormous dilution effect of the meltwater with respect to e.g. salinity, alkalinity, and carbon content, which could comply with the observed alkaline pH observed for the onset of cap carbonate deposition. The resulting pCO_2 disequilibrium between seawater and atmosphere causes enhanced oceanic CO_2 uptake inducing an ocean acidification. Again this could be comparable to the observed transition pattern into ocean

acidification during cap carbonate deposition in the Marinoan aftermath. CO_2 uptake would continue until the ocean reaches equilibrium and ocean acidification would be sustained until the climate is regulated by CO_2 draw down.

ISOCHRONOUS VS DIACHRONOUS CAP CARBONATE DEPOSITION

Hoffman et al. (2007) argue that sedimentary structures as well as the carbon isotope record from the platform to the lower slope in Namibia support a diachronous deposition of post-glacial cap carbonates. This is based on the observation that the overall sigmoidal trajectory of the carbon isotope signal is only incompletely sampled in any single section. If so, then the boron isotope signal should reveal similar incomplete sigmoidal trajectories across the basin. This is, however, not the case since our data show rather complete and synchronous pattern. In view of a potential meltwater plume after deglaciation, the B isotope profiles would fit the semi-diachronous model promoted by Shields (2005). Initially, cap dolostones, in our case the basal laminated Keilberg dolostone, are deposited under the, for example, influence of an incipient meltwater plume above the deeper water setting. As the plume grows it floods the bank such that the interval of ocean acidification is then largely captured within the upper Keilberg dolostone deposits. By the time of Maieberg limestone deposition, the pH of the seawater on the platform is buffered by local changes in alkalinity i.e. continental weathering. This scenario is compatible with the conditions hypothesized by Shields (2005). An isochronous or semi-diachronous model for cap dolomite deposition is also suggested for additional palaeo-continents: Mongolia and South Australia (Liu et al., 2014).

While our boron isotope record from the platform to the lower slope supports a synchronous or semi-diachronous cap carbonate deposition model, we nevertheless cannot completely rule out the possibility of a diachronous model.

REFERENCES

Alexeiev, D. V., Cook, H. E., Buvtyshkin, V. M., and Golub, L. Y., 2009, Structural evolution of the Ural-Tian Shan junction: A view from Karatau ridge, South Kazakhstan: Comptes Rendus Geosciences, v. 341, no. 2-3, p. 287-297.

Allen, M. B., Alsop, G. I., and Zhemchuzhnikov, V. G., 2001, Dome and basin refolding and transpressive inversion along the Karatau Fault System, southern Kazakstan: Journal of the Geological Society, v. 158, no. 1, p. 83-95.

Anbar, A. D., and Knoll, A. H., 2002, Proterozoic Ocean Chemistry and Evolution: A Bioinorganic Bridge?: Science, v. 297, no. 5584, p. 1137-1142.

Bates, N. R., Garley, R., Frey, K. E., Shake, K. L., and Mathis, J. T., 2014, Sea-ice melt CO2-carbonate chemistry in the western Arctic Ocean: meltwater contributions to air-sea CO2 gas exchange, mixed layer properties and rates of net community production under sea ice: Biogeosciences Discuss., v. 11, no. 1, p. 1097-1145.

Condon, D., Zhu, M., Bowring, S., Wang, W., Yang, A., and Jin, Y., 2005, U-Pb Ages from the Neoproterozoic Doushantuo Formation, China: Science, v. 308, no. 5718, p. 95-98.

Cook, H. E., Johnson, P. D., Matti, J. C., and Zemmels, I., 1975, Methods of sample preparation and X-ray diffraction data analysis, X-ray Mineralogy Laboratory, Deep Sea Drilling Project, University of California, Riverside: In: Hayes, D.E., Frakes, L.A., et al., Init. Repts.

Derkowski, A., Bristow, T. F., Wampler, J. M., Środoń, J., Marynowski, L., Elliott, W. C., and Chamberlain, C. P., 2013, Hydrothermal alteration of the Ediacaran Doushantuo Formation in the Yangtze Gorges area (South China): Geochimica et Cosmochimica Acta, v. 107, no. 0, p. 279-298.

Derry, L. A., 2010, A burial diagenesis origin for the Ediacaran Shuram–Wonoka carbon isotope anomaly: Earth and Planetary Science Letters, v. 294, no. 1-2, p. 152-162.

Derry, L. A., Kaufman, A. J., and Jacobsen, S. B., 1992, Sedimentary cycling and environmental change in the Late Proterozoic: Evidence from stable and radiogenic isotopes: Geochimica et Cosmochimica Acta, v. 56, no. 3, p. 1317-1329.

296 Dickson, A. G., 1990, Thermodynamics of the dissociation of boric acid in synthetic seawater from
297 273.15 to 318.15 K: Deep Sea Research Part A. Oceanographic Research Papers, v. 37, no. 5,
298 p. 755-766.
299 Doney, S. C., 2006, The Dangers of Ocean Acidification: Scientific American, v. 294, p. 58-65.
300 Eganov, E. A., Ergaliev, G. K., Ilyin, A. V., and Krasnov, A. A., 1984, Guidebook / International
301 Geological Congress, XXVII Session Kazakhstan: Karatau Phosphorite Basin, Moskau,
302 Nauka.
303 Eganov, E. A., Sovetov, Y. K., and Yanshin, A. L., 1986, Proterozoic and Cambrian phosphorite
304 deposits: Karatau, southern Kazakhstan, USSR: In: Cook, P.J., Shergold, J.H. (Eds.),
305 Phosphate Deposits of the World: Volume 1 Proterozoic and Cambrian Phosphorites.
306 Cambridge University Press, Cambridge, UK, p. 175-189.
307 Feely, R. A., and Kleypas, J., 2012, *in* Cooley, S., Mathis, J., Yates, K., Turley, C., Frequently Asked
308 Questions about Ocean Acidification, ed.: U.S. Ocean Carbon and Biogeochemistry Program
309 and the UK Ocean Acidification Research Programme, Version 2, www.whoi.edu/OCB-
310 OA/FAQs.
311 Foster, G. L., Pogge von Strandmann, P. A. E., and Rae, J. W. B., 2010, Boron and magnesium
312 isotopic composition of seawater: Geochemistry, Geophysics, Geosystems, v. 11.
313 Grotzinger, J. P., and Kasting, J. F., 1993, New Constraints on Precambrian Ocean Composition: The
314 Journal of Geology, v. 101, no. 2, p. 235-243.
315 Hare, A. A., Wang, F., Barber, D., Geilfus, N. X., Galley, R. J., and Rysgaard, S., 2013, pH evolution
316 in sea ice grown at an outdoor experimental facility: Marine Chemistry, v. 154, p. 46-54.
317 Hemming, N. G., and Hanson, G. N., 1992, Boron isotopic composition and concentration in modern
318 marine carbonates: Geochimica et Cosmochimica Acta, v. 56, no. 1, p. 537-543.
319 Higgins, J. A., and Schrag, D. P., 2003, Aftermath of a snowball Earth: Geochemistry, Geophysics,
320 Geosystems, v. 4, no. 3, p. 1028.
321 Hoffman, P. F., Halverson, G. P., Domack, E. W., Husson, J. M., Higgins, J. A., and Schrag, D. P.,
322 2007, Are basal Ediacaran (635 Ma) post-glacial “cap dolostones” diachronous?: Earth and
323 Planetary Science Letters, v. 258, no. 1–2, p. 114-131.

Hoffman, P. F., Hawkins, D. P., Isachsen, C. E., and Bowring, S. A., 1996, Precise U-Pb zircon ages for early Damaran magmatism in the Summas Mountains and Welwitschia Inlier, northern Damara Belt, Namibia: Communications of the Geological Survey of Namibia, v. 11, p. 47-52.

Hoffman, P. F., and Li, Z.-X., 2009, A palaeogeographic context for Neoproterozoic glaciation: Palaeogeography, Palaeoclimatology, Palaeoecology, v. 277, no. 3–4, p. 158-172.

Hoffmann, K.-H., Condon, D. J., Bowring, S. A., and Crowley, J. L., 2004, U-Pb zircon date from the Neoproterozoic Ghaub Formation, Namibia: Constraints on Marinoan glaciation: Geology, v. 32, no. 9, p. 817-820.

Hofmann, G. E., Smith, J. E., Johnson, K. S., Send, U., Levin, L. A., Micheli, F., Paytan, A., Price, N. N., Peterson, B., Takeshita, Y., Matson, P. G., Crook, E. D., Kroeker, K. J., Gambi, M. C., Rivest, E. B., Frieder, C. A., Yu, P. C., and Martz, T. R., 2011, High-Frequency Dynamics of Ocean pH: A Multi-Ecosystem Comparison: Plos One, v. 6, no. 12.

Jacobsen, S. B., and Kaufman, A. J., 1999, The Sr, C and O isotopic evolution of Neoproterozoic seawater: Chemical Geology, v. 161, no. 1–3, p. 37-57.

Jiang, G., Kennedy, M. J., and Christie-Blick, N., 2003, Stable isotopic evidence for methane seeps in Neoproterozoic postglacial cap carbonates: Nature, v. 426, no. 6968, p. 822-826.

Joachimski, M. M., Simon, L., van Geldern, R., and Lécuyer, C., 2005, Boron isotope geochemistry of Paleozoic brachiopod calcite: Implications for a secular change in the boron isotope geochemistry of seawater over the Phanerozoic: Geochimica et Cosmochimica Acta, v. 69, no. 16, p. 4035-4044.

Kakihana, H., Kotaka, M., Satoh, S., Nomura, M., and Okamoto, M., 1977, Fundamental Studies on the Ion-Exchange Separation of Boron Isotopes: Bulletin of the Chemical Society of Japan, v. 50, no. 1, p. pp.158-163.

Kasemann, S. A., Hawkesworth, C. J., Prave, A. R., Fallick, A. E., and Pearson, P. N., 2005, Boron and calcium isotope composition in Neoproterozoic carbonate rocks from Namibia: evidence for extreme environmental change: Earth and Planetary Science Letters, v. 231, no. 1-2, p. 73-86.

352 Kasemann, S. A., Meixner, A., Rocholl, A., Vennemann, T., Rosner, M., Schmitt, A. K., and
353 Wiedenbeck, M., 2001, Boron and Oxygen Isotope Composition of Certified Reference
354 Materials NIST SRM 610/612 and Reference Materials JB-2 and JR-2: Geostandards
355 Newsletter, v. 25, no. 2-3, p. 405-416.
356 Kasemann, S. A., Prave, A. R., Fallick, A. E., Hawkesworth, C. J., and Hoffmann, K.-H., 2010,
357 Neoproterozoic ice ages, boron isotopes, and ocean acidification: Implications for a snowball
358 Earth: Geology, v. 38, no. 9, p. 775-778.
359 Kasemann, S. A., Schmidt, D. N., Bijma, J., and Foster, G. L., 2009, In situ boron isotope analysis in
360 marine carbonates and its application for foraminifera and palaeo-pH: Chemical Geology, v.
361 260, no. 1-2, p. 138-147.
362 Kaufman, A. J., Hayes, J. M., Knoll, A. H., and Germs, G. J. B., 1991, Isotopic composition of
363 carbonates and organic-carbon from upper Proterozoic successions in Namibia - Stratigraphic
364 variation and the effects of diagenesis and metamorphism: Precambrian Research, v. 49, no. 3-
365 4, p. 301-327.
366 Kaufman, A. J., Jacobsen, S. B., and Knoll, A. H., 1993, The Vendian record of Sr and C isotopic
367 variations in seawater: Implications for tectonics and paleoclimate: Earth and Planetary
368 Science Letters, v. 120, no. 3–4, p. 409-430.
369 Kempe, S., and Kazmierczak, J., 2002, Biogenesis and Early Life on Earth and Europa: Favored by an
370 Alkaline Ocean?: Astrobiology, v. 2, no. 1, p. 123-130.
371 Kisakurek, B., James, R. H., and Harris, N. B. W., 2005, Li and [delta]7Li in Himalayan rivers:
372 Proxies for silicate weathering?: Earth and Planetary Science Letters, v. 237, no. 3-4, p. 387-
373 401.
374 Klochko, K., Kaufman, A. J., Yao, W., Byrne, R. H., and Tossell, J. A., 2006, Experimental
375 measurement of boron isotope fractionation in seawater: Earth and Planetary Science Letters,
376 v. 248, no. 1-2, p. 276-285.
377 Larose, C., Dommergue, A., De Angelis, M., Cossa, D., Averty, B., Marusczak, N., Soumis, N.,
378 Schneider, D., and Ferrari, C., 2010, Springtime changes in snow chemistry lead to new

379 insights into mercury methylation in the Arctic: Geochimica et Cosmochimica Acta, v. 74, no.
380 22, p. 6263-6275.
381 Le Hir, G., Donnadieu, Y., Goddéris, Y., Pierrehumbert, R. T., Halverson, G. P., Macouin, M.,
382 Nédélec, A., and Ramstein, G., 2009, The snowball Earth aftermath: Exploring the limits of
383 continental weathering processes: Earth and Planetary Science Letters, v. 277, no. 3–4, p. 453-
384 463.
385 Lemarchand, D., Gaillardet, J., Lewin, E., and Allegre, C. J., 2000, The influence of rivers on marine
386 boron isotopes and implications for reconstructing past ocean pH: Nature, v. 408, no. 6815, p.
387 951-954.
388 Li, Z.-X., Evans, D. A. D., and Halverson, G. P., 2013, Neoproterozoic glaciations in a revised global
389 palaeogeography from the breakup of Rodinia to the assembly of Gondwanaland: Sedimentary
390 Geology, v. 294, no. 0, p. 219-232.
391 Liu, C., Wang, Z., and Raub, T. D., 2013, Geochemical constraints on the origin of Marinoan cap
392 dolostones from Nuccaleena Formation, South Australia: Chemical Geology, v. 351, no. 0, p.
393 95-104.
394 Liu, C., Wang, Z., Raub, T. D., Macdonald, F. A., and Evans, D. A. D., 2014, Neoproterozoic cap-
395 dolostone deposition in stratified glacial meltwater plume: Earth and Planetary Science
396 Letters, v. 404, no. 0, p. 22-32.
397 Ma, G., Li, H., and Zhang, Z., 1984, An investigation of the age limits of the Sinian System in South
398 China: Bulletin of Yichang Institute of Geology Mineral Resources, v. 8, p. 1-29.
399 Meert, J. G., Gibsher, A. S., Levashova, N. M., Grice, W. C., Kamenov, G. D., and Ryabinin, A. B.,
400 2011, Glaciation and ~ 770 Ma Ediacara (?) Fossils from the Lesser Karatau Microcontinent,
401 Kazakhstan: Gondwana Research, v. 19, no. 4, p. 867-880.
402 Miller, N. R., Stern, R. J., Avigad, D., Beyth, M., and Schilman, B., 2009, Cryogenian slate-carbonate
403 sequences of the Tambien Group, Northern Ethiopia (I): Pre-“Sturtian” chemostratigraphy and
404 regional correlations: Precambrian Research, v. 170, no. 3–4, p. 129-156.
405 Miller, R. M., 2008, The geology of Namibia: Palaeozoic to Cenozoic, Windhoek, Geological Survey,
406 Namibia.

407 Palmer, M. R., Spivack, A. J., and Edmond, J. M., 1987, Temperature and pH controls over isotopic
408 fractionation during adsorption of boron on marine clay: Geochimica et Cosmochimica Acta,
409 v. 51, no. 9, p. 2319-2323.
410 Paris, G., Bartolini, A., Donnadieu, Y., Beaumont, V., and Gaillardet, J., 2010, Investigating boron
411 isotopes in a middle Jurassic micritic sequence: Primary vs. diagenetic signal: Chemical
412 Geology, v. 275, no. 3-4, p. 117-126.
413 Pearson, P. N., and Palmer, M. R., 2000, Atmospheric carbon dioxide concentrations over the past 60
414 million years: Nature, v. 406, no. 6797, p. 695-699.
415 Raub, T. D., Evans, D. A. D., and Smirnov, A. V., 2007, Siliciclastic prelude to Elatina–Nuccaleena
416 deglaciation: lithostratigraphy and rock magnetism of the base of the Ediacaran system:
417 Geological Society, London, Special Publications, v. 286, no. 1, p. 53-76.
418 Sanyal, A., Nugent, M., Reeder, R. J., and Bijma, J., 2000, Seawater pH control on the boron isotopic
419 composition of calcite: evidence from inorganic calcite precipitation experiments: Geochimica
420 et Cosmochimica Acta, v. 64, no. 9, p. 1551-1555.
421 Shields, G. A., 2005, Neoproterozoic cap carbonates: a critical appraisal of existing models and the
422 plumeworld hypothesis: Terra Nova, v. 17, no. 4, p. 299-310.
423 Singh, V., Ramanathan, A. L., Pottakkal, J., Sharma, P., Linda, A., Azam, M., and Chatterjee, C.,
424 2012, Chemical characterisation of meltwater draining from Gangotri Glacier, Garhwal
425 Himalaya, India: Journal of Earth System Science, v. 121, no. 3, p. 625-636.
426 Spivack, A. J., 1986, Boron isotope geochemistry [Ph.D.: Massachusetts Institute of Technology], 184
427 p.
428 Spivack, A. J., and Edmond, J. M., 1987, Boron isotope exchange between seawater and the oceanic
429 crust: Geochimica et Cosmochimica Acta, v. 51, no. 5, p. 1033-1043.
430 Spivack, A. J., and You, C.-F., 1997, Boron isotopic geochemistry of carbonates and pore waters,
431 Ocean Drilling Program Site 851: Earth and Planetary Science Letters, v. 152, no. 1–4, p. 113-
432 122.
433 Takahashi, T., Sutherland, S. C., Chipman, D. W., Goddard, J. G., Ho, C., Newberger, T., Sweeney,
434 C., and Munro, D. R., 2014, Climatological distributions of pH, pCO2, total CO2, alkalinity,

435 and CaCO3 saturation in the global surface ocean, and temporal changes at selected locations:
436 Marine Chemistry, v. 164, no. 0, p. 95-125.
437 Tegt, S. K., 2002, The chemical evolution of Canada glacier melt: Supraglacial and proglacial waters
438 in Taylor Valley Antartica [M.S.: The Ohio State University, 149 p.
439 Veizer, J., Ala, D., Azmy, K., Bruckschen, P., Buhl, D., Bruhn, F., Carden, G. A. F., Diener, A.,
440 Ebneth, S., Godderis, Y., Jasper, T., Korte, C., Pawellek, F., Podlaha, O. G., and Strauss, H.,
441 1999, 87Sr/86Sr, δ13C and δ18O evolution of Phanerozoic seawater: Chemical Geology, v.
442 161, no. 1–3, p. 59-88.
443 Vogl, J., Rosner, M., and Pritzkow, W., 2011, Development and validation of a single collector SF-
444 ICPMS procedure for the determination of boron isotope ratios in water and food samples:
445 Journal of Analytical Atomic Spectrometry, v. 26, no. 4, p. 861-869.
446 Wimpenny, J., James, R. H., Burton, K. W., Gannoun, A., Mokadem, F., and Gíslason, S. R., 2010,
447 Glacial effects on weathering processes: New insights from the elemental and lithium isotopic
448 composition of West Greenland rivers: Earth and Planetary Science Letters, v. 290, no. 3–4, p.
449 427-437.
450 Xiao, S., McFadden, K. A., Peek, S., Kaufman, A. J., Zhou, C., Jiang, G., and Hu, J., 2012, Integrated
451 chemostratigraphy of the Doushantuo Formation at the northern Xiaofenghe section (Yangtze
452 Gorges, South China) and its implication for Ediacaran stratigraphic correlation and ocean
453 redox models: Precambrian Research, v. 192-195, no. 0, p. 125-141.
454 Zhang, J. M., Li, G., Zhou, C. M., Zhu, M. Y., and Yu, Z., 1997, Carbon isotope profiles and their
455 correlation across the Neoproterozoic-Cambrian boundary interval on the Yangtze Platform,
456 China: Bulletin of National Museum of Natural Science, v. 10, p. 107-116.
457 Zhu, M. Y., Zhang, J., Steiner, M., Yang, A., Li, G., and Erdtmann, B.-D., 2003, Sinian-Cambrian
458 stratigraphic framework for shallow-to-deep-water environments of the Yangtze Platform: an
459 integrated approach: Progress in Natural Science, v. 13, no. 12, p. 951-960.

460

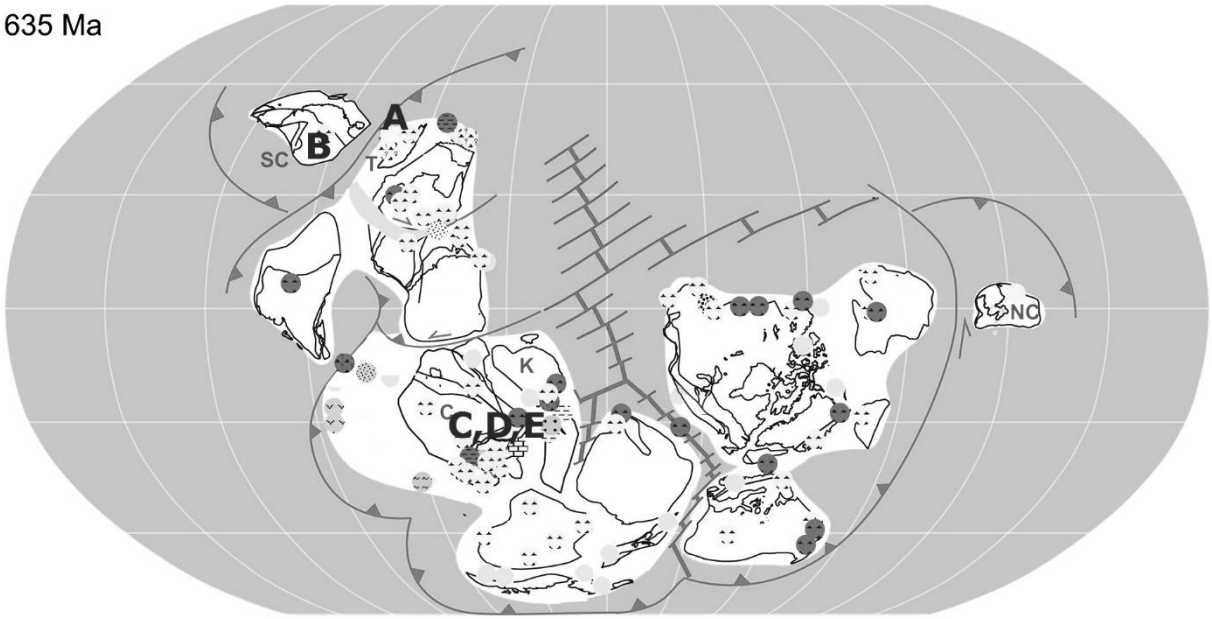

461

462 Figure DR1: Palaeogeographic reconstruction for 635 Ma (slightly modified from Li et al.,
463 2013). The investigated sections are indicated in black: A: Kyrshabakty Section, Karatau
464 microcontinent. B: N Xiaofenghe Section, South China Block. C: Ombaatjie Section, Congo
465 craton. D: Khowarib Section, Congo craton. E: Fransfontein Section, Congo craton. The
466 geographic position of the Karatau-Naryn terrane is suggested to be close to South China and
467 the Tarim microcontinent. Abbreviations of the terranes: C-Congo; K-Kalahari; NC-North
468 China; SC-South China; T-Tarim.

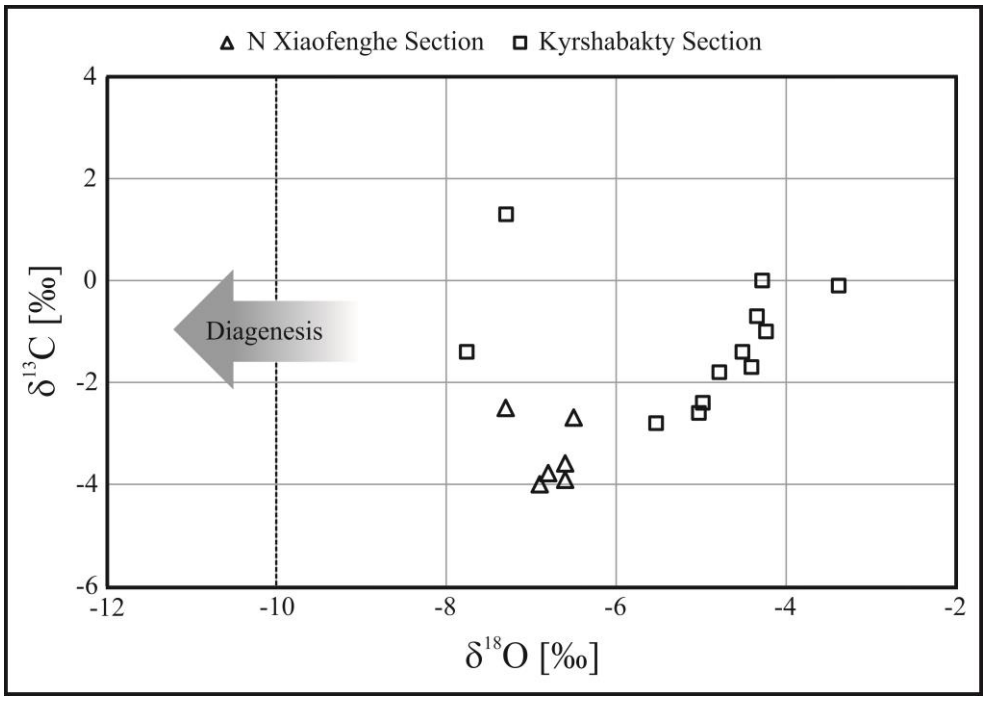

Figure DR2: Cross-plot of $\delta^{13}C_{carb}$ vs. $\delta^{18}O$ data of the Northern Xiaofenghe (triangles) and Kyrshabakty Section (squares). No data are in the diagenesis-field and no significant correlation is obvious.

Assumptions for pH calculations: $pK_{B} =$ 8.579 Dickson, 1990

$\alpha =$ 1.0272 Klochko *et al.*, 2006

A: **20.5‰** $\delta^{11}B_{seawater}$

B: **21.5‰** $\delta^{11}B_{seawater}$

C: **22.5‰** $\delta^{11}B_{seawater}$

China Yangtze Platform								
N. Xiaofenghe Section		$\delta^{13}C$	$\delta^{18}O$	$\delta^{11}B$		A	B	C
Sample	meter	[‰]	[‰]	[‰]	2σ	pH	pH	pH
NXF0.2	0.2	-4.0	-6.9	9.6	0.1	8.8	8.7	8.6
NXF0.75	0.8	-3.6	-6.6	6.8	1.3	8.6	8.5	8.5
NXF1.6	1.6	-3.8	-6.8	-2.2	1.6	7.9	7.8	7.6
NXF2.35B	2.4	-3.9	-6.6	4.8	0.2	8.5	8.4	8.3
NXF3.85	3.9	-2.7	-6.5	5.4	0.0	8.5	8.4	8.4
NXF4.8	4.8	-2.5	-7.3	13.5	1.1	9.1	9.0	8.9
NXF6.65	6.7	-0.2	n.a.	14.8	0.1	9.2	9.1	9.0
NXF22	22.0	1.8	n.a.	n.a.				
Kazakhstan Malyi Karatau Range								
Kyrshabakty Section		$\delta^{13}C$	$\delta^{18}O$	$\delta^{11}B$		A	B	C
Sample	meter	[‰]	[‰]	[‰]	2σ	pH	pH	pH
KY 3	0.0	-0.1	-3.4	8.7	0.2	8.7	8.7	8.6
KY 4	0.2	-0.7	-4.3	6.5	1.2	8.6	8.5	8.4
KY 5a	0.4	-1.4	-4.5	6.5	1.6	8.6	8.5	8.4
KY 5b	0.5	-1.8	-4.8	8.2	0.2	8.7	8.6	8.6
KY 6a	0.8	n.a.	n.a.	6.1	1.0	8.6	8.5	8.4
KY 6b	0.9	-1.7	-4.4	2.9	0.2	8.3	8.3	8.2
KY 7a	1.3	-2.4	-5.0	1.7	0.8	8.2	8.2	8.1
KY 7b	1.3	-2.8	-5.5	5.6	0.3	8.5	8.5	8.4
KY 8	2.1	-1.3	n.a.	6.2	1.0	8.6	8.5	8.4
KY 9	3.2	-2.6	-5.0	7.3	0.0	8.6	8.6	8.5
KY 10	3.5	-1.0	-4.2	8.1	0.3	8.7	8.6	8.6
KY 10a	8.6	-1.4	-7.8	13.8	0.8	9.1	9.0	8.9
KY 11	19.3	0.0	-4.3	14.2	0.2	9.1	9.0	9.0
KY 13	29.5	1.3	-7.3	7.8	0.7	8.7	8.6	8.5
Namibia Congo Craton								
Khowarib Section		$\delta^{13}C$	$\delta^{18}O$	$\delta^{11}B$*		A	B	C
Sample	meter	[‰]	[‰]	[‰]		pH	pH	pH
KW1-10	0.0	-3.2	-7.4	9.7		8.8	8.7	8.7
KW1-11	0.1	-3.2	-7.3	6.7		8.6	8.5	8.5
KW1-12	0.2	-3.2	-6.1	3.2		8.4	8.3	8.2
KW1-14	0.6	-3.0	-7.2	2.8		8.3	8.3	8.2
KW1-15	0.8	n.a.	n.a.	3.5		8.4	8.3	8.2
KW1-18	1.4	-3.1	-7.7	1.7		8.2	8.2	8.1
KW1-18	1.4	-3.1	-7.7	1.5		8.2	8.2	8.1
KW1-21	2.7	-2.9	-7.6	2.0		8.3	8.2	8.1
KW1-24	4.3	-3.0	-7.7	1.5		8.2	8.2	8.1
KW1-29	6.8	-2.8	-7.5	2.7		8.3	8.3	8.2

KW1-32	8.3	-3.0	-7.5	-0.1	8.1	8.0	7.9
KW1-37	10.8	-3.3	-6.9	-1.2	8.0	7.9	7.8
KW1-45	14.8	-4.2	-9.0	0.5	8.2	8.1	8.0
KW1-55	21.3	-5.1	-8.6	2.2	8.3	8.2	8.1
KW1-58	31.3	-5.2	-9.1	0.2	8.1	8.0	7.9
KW1-64	57.3	-5.2	-9.6	3.2	8.4	8.3	8.2
KW1-67	80.3	-5.2	-9.5	2.5	8.3	8.2	8.2
Namibia	Congo Craton						
Fransfontein Section		$\delta^{13}C$	$\delta^{18}O$	$\delta^{11}B$*	A	B	C
Sample	meter	[‰]	[‰]	[‰]	pH	pH	pH
FF1-2	0.2	-1.6	-7.0	3.0	8.3	8.3	8.2
FF1-3	0.4	-1.8	-7.0	1.2	8.2	8.1	8.0
FF1-4	0.6	-2.2	-7.3	-0.5	8.1	8.0	7.9
FF1-5	0.8	-1.7	-6.7	-1.2	8.0	7.9	7.8
FF1-6	1.0	-2.6	-7.3	-2.6	7.8	7.7	7.5
FF1-9	1.6	-2.3	-7.4	1.0	8.2	8.1	8.0
FF1-12	2.2	-3.0	-7.5	-2.2	7.9	7.8	7.6
FF1-20	4.6	-3.3	-8.3	-3.5	7.7	7.5	7.2
FF1-22	5.4	-2.8	-8.8	n.a.			
FF1-28	14.7	-4.1	-10.2	-3.6	7.7	7.5	7.2
FF1-29	42.0	-4.4	-9.7	-2.0	7.9	7.8	7.6
FF1-30	42.7	-4.2	-9.4	-2.5	7.9	7.7	7.5
FF1-31	48.2	-0.3	-6.9	-4.3	7.6	7.3	6.6
FF1-32	52.2	0.6	-5.3	-1.0	8.0	7.9	7.8
FF1-34	72.2	1.5	-1.5	2.0	8.3	8.2	8.1
FF1-36	92.2	1.6	-0.9	4.5	8.4	8.4	8.3
FF1-37	102.2	1.6	-5.0	6.7	8.6	8.5	8.5
Namibia	Congo Craton						
Ombaatjie Section		$\delta^{13}C$	$\delta^{18}O$	$\delta^{11}B$*	A	B	C
Sample	meter	[‰]	[‰]	[‰]	pH	pH	pH
OBTJ 43	0.1	1.7	-4.6	2.7	8.3	8.3	8.2
OBTJ 45	1.5	-2.6	-6.3	-3.3	7.7	7.6	7.3
OBTJ 46	1.6	-2.6	-6.9	-5.5	7.2	5.9	-
OBTJ 47	2.5	-3.0	-6.9	-4.8	7.4	7.1	-
OBTJ 52	5.6	-3.0	-6.8	-6.2	6.7	-	-
OBTJ 55	10.5	-3.9	-8.5	-6.0	6.9	-	-
OBTJ 58	36.0	-5.8	-11.4	-2.4	7.9	7.7	7.6
OBTJ 65	106.0	-4.1	-8.9	-0.2	8.1	8.0	7.9

Table DR1: Boron ($\delta^{11}B$ [‰, vs. NIST SRM 951]), carbonate carbon ($\delta^{13}C_{carb}$ [‰, vs. VPDB]) and oxygen ($\delta^{18}O$ [‰, vs. VPDB]) isotope data of all analyzed sections, including Namibia data (Kasemann et al., 2010). Uncertainty for Namibian B isotope data is $\delta^{11}B$*: ±1‰ $2\sigma_f$. A, B, C are pH estimations based on different $\delta^{11}B_{seawater}$ assumptions: pK_B of 8.579 (Dickson, 1990), a fractionation factor α of 1.0272 (Klochko et al., 2006) and a seawater $\delta^{11}B$ composition of

A=20.5‰, B=21.5‰ and C=22.5‰ (same as Kasemann et al. (2010)) are used. The finally proposed $\delta^{11}B_{sw}$ composition of 20.5‰ is shaded in grey. n.a. = not analyzed.

Section	Height/ Sample	Al μg g^{-1}	B μg g^{-1}	Fe μg g^{-1}	Mn μg g^{-1}	S μg g^{-1}	Si μg g^{-1}	Sr μg g^{-1}	Ca %	Mg %
NXF	0.20	176	2	3763	2768	89	205	92	28	15
NXF	0.75	219	2	8813	2891	92	185	66	28	15
NXF	1.60	331	2	3348	1788	116	482	71	30	13
NXF	2.35	157	2	4574	2591	83	232	80	29	14
NXF	3.85	873	3	3320	2598	401	2243	87	32	12
NXF	4.80	158	3	11678	7065	90	193	64	28	15

Table DR2: Major and trace elements for the Chinese Xiaofenghe Section (NXF).